Growth Mechanism and Controlled Synthesis of AB-Stacked Bilayer Graphene on Cu–Ni Alloy Foils

Yaping Wu,[†,‡] Harry Chou,[†] Hengxing Ji,[†] Qingzhi Wu,[†] Shanshan Chen,[†] Wei Jiang,[‡] Yufeng Hao,[†] Junyong Kang,[‡] Yujie Ren,[†] Richard D. Piner,[†] and Rodney S. Ruoff[†,*]

[†]Department of Mechanical Engineering and the Materials Science and Engineering Program, The University of Texas at Austin, Austin, Texas 78712, United States and [‡]Department of Physics, Xiamen University, Xiamen 361005, People's Republic of China

ABSTRACT

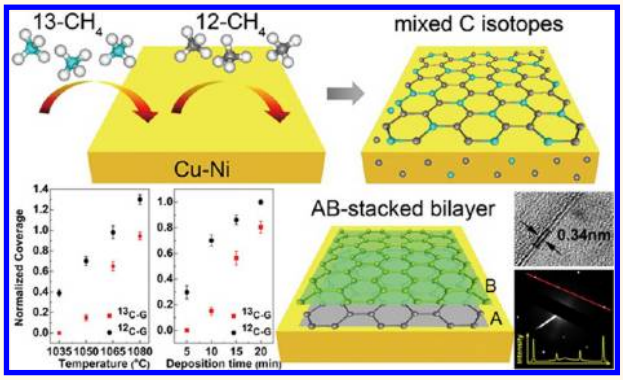

Strongly coupled bilayer graphene (*i.e.*, AB stacked) grows particularly well on commercial "90–10" Cu–Ni alloy foil. However, the mechanism of growth of bilayer graphene on Cu–Ni alloy foils had not been discovered. Carbon isotope labeling (sequential dosing of $^{12}CH_4$ and $^{13}CH_4$) and Raman spectroscopic mapping were used to study the growth process. It was learned that the mechanism of graphene growth on Cu–Ni alloy is by precipitation at the surface from carbon dissolved in the bulk of the alloy foil that diffuses to the surface. The growth parameters were varied to investigate their effect on graphene coverage and isotopic composition. It was found that higher temperature, longer exposure time, higher rate of bulk diffusion for ^{12}C *vs* ^{13}C, and slower cooling rate all produced higher graphene coverage on this type of Cu–Ni alloy foil. The isotopic composition of the graphene layer(s) could also be modified by adjusting the cooling rate. In addition, large-area, AB-stacked bilayer graphene transferrable onto Si/SiO_2 substrates was controllably synthesized.

KEYWORDS: Cu–Ni alloy · carbon isotopes · growth mechanism · AB-stacked bilayer graphene · Raman · TOF-SIMS · TEM

Graphene is a two-dimensional (2D) monolayer of carbon atoms.[1,2] Since being identified in 1969,[3] it has revealed a cornucopia of enticing properties, such as the ballistic transport and quantum Hall effect, which make it a promising candidate for future electronic applications.[2,4–6] In addition, AB-stacked bilayer graphene is of interest to microelectronics owing to its tunable band structure.[7,8] The bandgap can be tuned up to 250 mV by a perpendicular electric field, which is useful in various devices such as tunneling field-effect transistors and tunable laser diodes.[7,9,10] Prototype graphene transistors, with an on/off ratio exceeding 100 at room temperature, have been successfully fabricated by using AB-stacked bilayer graphene obtained by mechanical exfoliation of graphite.[9] However, the mechanical exfoliation method is time-consuming and unsuitable for industrial applications.

Chemical vapor deposition (CVD) of hydrocarbons on metal substrates, especially Ni and Cu, is a promising and versatile technique to synthesize large-area, high quality graphene sheets that are transferrable onto dielectric substrates.[11–15] Pure Ni foils usually generate graphene films with small domains and variable thickness across the films.[13,16] Ni thin film with thickness of hundreds of nanometers on SiO_2 substrate was used for growing double-layer graphene, but the two layers were not AB-stacked. Cu and Cu–Mo alloy were reported as excellent for generating monolayer graphene, but these substrates were usually poor for bilayer and multilayer films, especially in AB-stacked, because of the self-terminating growth.[10,11,17] A two-step growth scheme was reported to yield bilayer domains on Cu;[9] however, the domain size was limited to around 20 μm. The difference in graphene growth on Ni and Cu is primarily due to the differing solubility of carbon, that is, about 1.3 atom % of carbon in Ni[18] but <0.001 atom % of carbon in Cu, at 1000 °C.[16,19,20] We evaluated commercial Cu–Ni alloy foils, which are available in two standard types, namely "90–10" (weight percent: 88.00% Cu, 9.90% Ni) and "70–30" (weight percent: 67.80% Cu, 31.00% Ni),[16] thus predominately Cu but with substantial Ni (and other elements as

* Address correspondence to r.ruoff@mail.utexas.edu.

Received for review April 17, 2012 and accepted August 25, 2012.

Published online 10.1021/nn301689m

well). Such metal foils find commercial use for example in ship-building, as the Ni (and other minority components) imbues the Cu with much greater resistance to corrosion, such as by salt water. With "70−30" Cu−Ni alloy foils we have synthesized large-area graphene and graphite thin films;[16] however, the growth mechanism was not fully understood, and the structure of the layer stacking was not previously studied. CVD growth of graphene on Ni occurs by precipitation from the bulk Ni, while growth on Cu at least for low pressure CVD appears to occur by surface mediated growth.[18] The relatively small Ni concentration in the "90−10" Cu−Ni alloy foil suggested to us the possibility of it potentially yielding high quality and large-area AB-stacked bilayer graphene.

In this work, carbon isotope labeling by sequential doping of unlabeled or ^{13}C-labeled methane, and Raman mapping, were used to probe the mechanism(s) of growth of monolayer and bilayer graphene on "90−10" Cu−Ni alloy foil. The effects of temperature, time, rates of diffusion for ^{12}C *vs* ^{13}C, and cooling rate, were systematically studied with an eye toward elucidating growth mechanism(s). High-quality, large-area monolayer and AB-stacked bilayer graphene were successfully achieved.

RESULTS AND DISCUSSION

Isotopic labeling was used to probe the growth mechanism of graphene on our Cu−Ni alloy foil. After annealing under 2 sccm H_2 at 1050 °C, 10 sccm normal methane ($^{12}CH_4$) and 10 sccm ^{13}C-labeled methane ($^{13}CH_4$) (methane partial pressure P_{Me} = 110 mTorr) were alternately input for 10 min each, and then the sample was cooled at a rate of 5 °C/min. Monolayer graphene was obtained with some adlayer islands. Only monolayer areas were chosen for the Raman analysis to avoid the coupling between layers which would impact the Raman shifts. A graphene domain that contains ^{12}C and ^{13}C at an atomic ratio of n_{12}/n_{13} gives Raman shifts at

$$\omega_i = \omega_{i,12}\sqrt{\frac{m_{12}}{n_{12}m_{12}+n_{13}m_{13}}} \quad (1)$$

where $\omega_{i,12}$ is the Raman shift of band i of ^{12}C-graphene, m_{12} and m_{13} are the atomic masses, and n_{12} and n_{13} are the atomic fractions of ^{12}C and ^{13}C, respectively.[18,21] Using this method, the local isotopic composition of graphene can be determined. We would expect graphene composed of pure ^{12}C- and ^{13}C-graphene domains with Raman shifts at ω_{12} and ω_{13}, respectively, if the film formed by surface mediated-growth. Alternatively, graphene domains containing a mixture of ^{12}C and ^{13}C, with a Raman shift of ω determined by eq 1, would be observed if the growth occurs by a segregation and/or the preciptation mechanism.[18,21]

Figure 1 panels a and b show an optical micrograph and a Raman map of the G peak position of a monolayer graphene transferred onto a SiO_2/Si substrate, respectively. The uniform contrast of the whole Raman map without distinguishable isotopic separation suggests that ^{12}C and ^{13}C are randomly distributed over the graphene film without either locally segregated. Figure 1c shows a typical Raman spectrum from the region in Figure 1b. The D, G, and 2D bands are located at the frequencies of 1330, 1565, and 2633 cm^{-1}, respectively, which indicates a mixture of 70% ^{12}C and 30% ^{13}C according to eq 1. These results suggest that the graphene film was formed though the surface precipitation of carbon diffusing out from the bulk,[18] and a schematic diagram visualizing the growth process and the distribution of carbon isotopes is shown in Figure 1d. To address the possibility that residual carbon impurities within the substrate could alter the precipitation process, two control experiments were performed. The results showed that the graphene growth observed here was not influenced by the residual carbon in the substrate (for details, see Supporting Information Figure S1).

To achieve a deeper understanding, growth conditions were varied to determine their effect on graphene growth. On the basis of the knowledge that the solubility of carbon changes with temperature, we first studied the influence of carbon-deposition temperature on the graphene growth. The samples were prepared at temperatures of 1035, 1050, 1060, and 1080 °C in 2 sccm H_2 and 10 sccm $^{12}CH_4$ (or $^{13}CH_4$) for 10 min, with a $^{12}CH_4$ (or $^{13}CH_4$) partial pressure of 110 mTorr and a cooling rate of 30 °C/min. Compared with the sample in Figure 1, a much faster cooling rate was used here to achieve submonolayer graphene coverage.[16]

Figure 2a−d shows the scanning electron microscopy (SEM) images of ^{13}C-graphene (left panel) and ^{12}C-graphene (right panel) on Cu−Ni alloy foils synthesized at various temperatures. The clear contrast differences show the graphene thickness, for example, 0, 1, and 2 layers.[11] The coverage of both ^{13}C-graphene and ^{12}C-graphene increases with temperature, because the solubility (N_c) and diffusivity (D_c) of carbon depend on the temperature as

$$N_c = N_c^0 \exp\left(\frac{-\Delta H^0}{RT}\right) \quad (2)$$

and

$$D_c = D_c^0 \exp\left(\frac{-Q_D}{RT}\right) \quad (3)$$

respectively. In these expressions, R is the universal gas constant, ΔH^0 is the partial molar enthalpy of solution for carbon, Q_D is the activation energy for diffusion, and N_c^0 and D_c^0 are the solubility and diffusion constants, respectively. These equations suggest that higher temperature enhances both the solubility and diffusivity of carbon in the alloy foil, thus greater graphene coverage was formed during the cooling process.

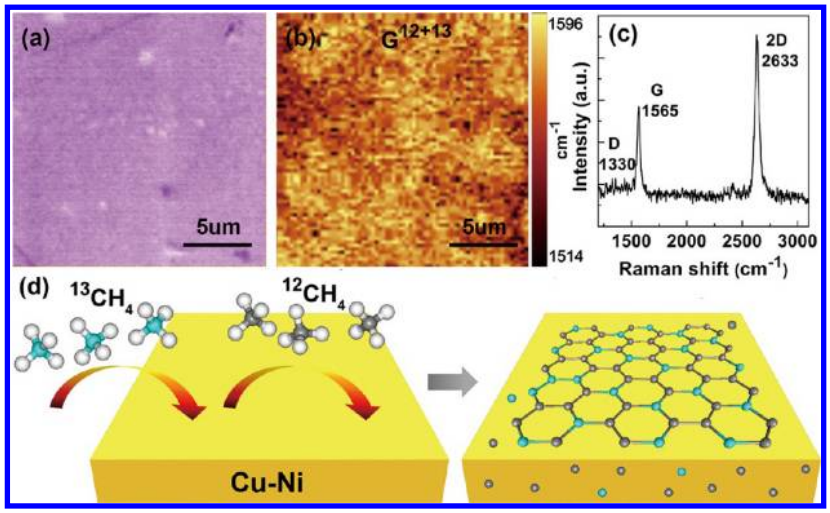

Figure 1. (a) Optical micrograph of a monolayer graphene transferred onto a 285 nm SiO_2/Si substrate. (b) The corresponding Raman map generated by the position of the G band (G^{12+13}, 1500−1650 cm^{-1}). (c) A Raman spectrum acquired from panel b. (d) Schematic diagrams of the growth process of carbon isotope labeled graphene, and the possible distribution of ^{12}C and ^{13}C atoms in graphene films and inside the Cu−Ni alloy. The gray and blue balls represent the ^{12}C and ^{13}C atoms, respectively.

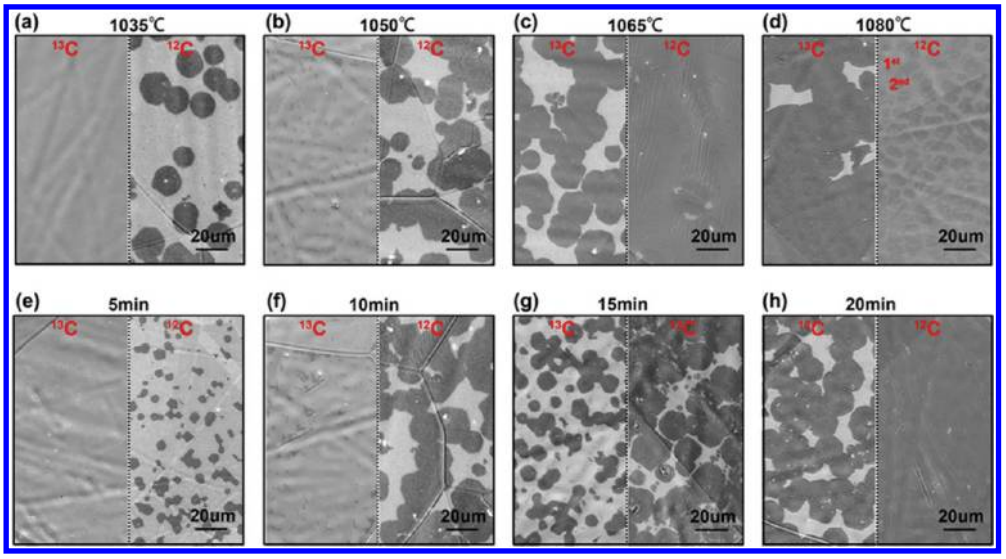

Figure 2. (a−d) SEM images of the ^{13}C-(left panel) and ^{12}C-graphene (right panel) on Cu−Ni alloy foils for a deposition time of 10 min and different deposition temperatures. (e−h) SEM images of the ^{13}C-graphene (left panel) and ^{12}C-graphene (right panel) on Cu−Ni alloy foils for a deposition temperature of 1050 °C and various exposure times.

In addition to the observation of temperature-dependent graphene coverage, ^{12}C-graphene exhibits a higher coverage than ^{13}C-graphene at all the exposure temperatures. For example, submonolayer ^{12}C-graphene is obtained at 1035 °C while no ^{13}C-graphene is observed (Figure 2a), and a full-coverage ^{12}C-graphene film with adlayers is obtained at 1080 °C but only a submonolayer of ^{13}C-graphene is obtained at the same temperature (Figure 2d).

It is also noted that longer carbon deposition time generates graphene with greater coverage. Figure 2 panels e−h show the SEM images of ^{13}C- and ^{12}C-graphene on the alloy foils obtained at a deposition temperature of 1050 °C and different deposition times. All other growth parameters were the same as the samples shown in Figure 2a−d. No graphene or only small graphene domains with around 5 μm in size (Figure 2e) are found with the exposure of alloy foils to $^{13}CH_4$ or $^{12}CH_4$, respectively, for 5 min. A significant increase in graphene domain size for $^{13}CH_4$ exposure for 20 min is observed (Figure 2h), and a completely covered, uniform monolayer graphene is formed for 20 min exposure of $^{12}CH_4$. A full-monolayer graphene film was transferred from the alloy surface onto a SiO_2/Si substrate, as shown in Figure 3a. The color contrast of the optical image is uniform, which means a uniform thickness of the graphene film. The quality and layer number were evaluated by Raman spectroscopy. As shown in Figure 3b, the D peak is almost undetectable compared with the intense G and 2D bands, indicating

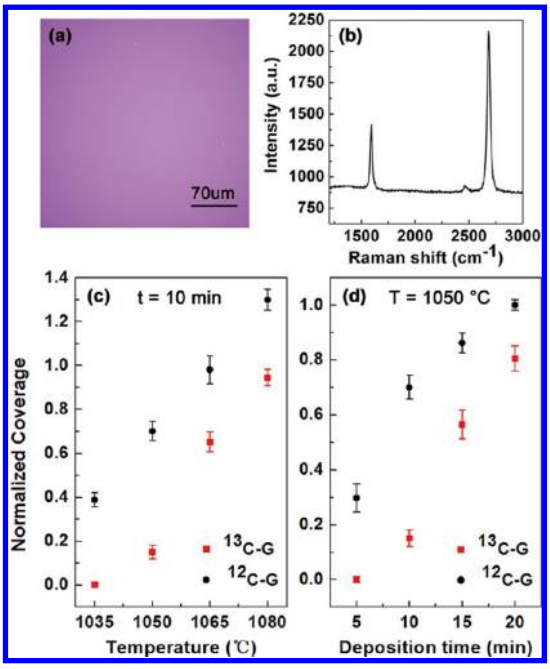

Figure 3. (a,b) Optical microscope image and a typical Raman spectrum taken from monolayer graphene transferred onto a 285 nm SiO_2/Si substrate; (c,(d) Normalized temperature-dependent and carbon-deposition-time-dependent coverage of ^{12}C- and ^{13}C-graphene, respectively. The error bars are generated by examining some SEM images at each growth condition.

the absence of a significant number of defects. The 2D band has a Lorentzian profile centered at 2678 cm^{-1} with a full width at half-maximum (fwhm) of 33 cm^{-1}, and the intensity ratio of G/2D is about 0.32. These features are typical of high-quality, monolayer graphene.

It is also notable from the SEM images in Figure 2 that the density of graphene islands increases with the growth temperature, and the average area of the islands steadily increases with exposure time. We studied several SEM images from each unique sample growth condition, and found that (1) the number of nucleating ^{12}C-graphene islands increases from about 23 to 34 per 10^5 μm^2 area when the growth temperature is raised from 1035 °C (Figure 2a) to 1050 °C (Figure 2b), while the lateral diameter of the islands only changes from around 14 to 15 μm; (2) at 1065 °C, the islands merge together and form a continuous layer (Figure 2c); (3) for ^{12}C-graphene, the average lateral diameter of the islands are around 5 μm (Figure 2e), 15 μm (Figure 2f) and 18 μm (Figure 2g) at growth times of 5, 10, and 15 min, respectively; (4) for ^{13}C-graphene, the island size extends from around 9 μm at 15 min (Figure 2g) to 17 μm at 20 min (Figure 2h). In other words, higher temperatures increase the graphene coverage mainly by producing more nucleation points, while longer exposure time increases the graphene coverage mainly by extending the size of each island.

The normalized graphene coverage with respect to the deposition temperatures and times are plotted numerically in Figure 3 panels c and d, respectively. The graphene coverage is determined by dividing the area of monolayer graphene by the total area captured in the SEM images. Thus, a coverage value of 1 is for a complete monolayer graphene film, <1 is for a submonolayer graphene film, and >1 is for a graphene film with adlayers. The coverage of ^{12}C-graphene was found to be 0.2−0.5 higher than that of ^{13}C-graphene at all of the growth conditions in this study.

Considering the evidence for precipitation growth of graphene on Cu−Ni alloy, the growth rate of graphene on Cu−Ni alloy should be proportional to the diffusion flux J per Fick's first law:[22]

$$J = -D(dC/dx) \quad (4)$$

where D is the diffusion coefficient, C is the concentration of carbon and x is the depth in the Cu−Ni alloy. Thus, the growth rate of graphene on Cu−Ni alloy is dominated by the diffusion coefficient and the concentration gradient of carbon. The diffusion coefficients of ^{12}C and ^{13}C in Cu−Ni alloy obey the classical relationship:

$$\frac{D_{12}}{D_{13}} = \left(\frac{m_{13}}{m_{12}}\right)^{1/2} \quad (5)$$

where D_{12} and D_{13} are the relevant diffusion coefficients, and m_{12} and m_{13} are the atomic masses of ^{12}C and ^{13}C atoms, respectively.[23−27] Hence, the diffusion coefficient of ^{12}C is about 4% higher than that of ^{13}C.

To probe the concentration gradient of carbon at the alloy surface, we used time-of-flight secondary ion mass spectrometry (TOF-SIMS), a surface analysis technique for chemical composition characterization, to track the distribution of carbon isotopes in the foils.[28,29] The ^{12}C and ^{13}C content in Cu−Ni alloy foil without carbon deposition were measured first (Figure 4a) to isolate any residual carbon influence. Samples in Figure 4b to 4e were grown at 1050 °C with a 2 sccm H_2 flow and a cooling rate of 30 °C/min under different methane flows. Samples 4b and 4c (shown in Figure 4b,c) were grown by introducing 10 sccm $^{12}CH_4$ and $^{13}CH_4$, respectively. Sample 4d (shown in Figure 4d) was prepared with 10 sccm $^{12}CH_4$ for 10 min and followed by 10 sccm $^{13}CH_4$ for an additional 10 min. Sample 4e (shown in Figure 4e) was prepared with the same conditions as sample 4d except the methane gas order was reversed. The depth profiles for the four samples shown in Figure 4b−e have had the background contents of ^{12}C and ^{13}C subtracted. In a comparison of samples 4b and 4c, the concentration of ^{12}C is higher near the surface, and gradually decreases into the foil, while the concentration of ^{13}C is initially lower and decreases steeply. These results reveal an isotope effect for carbon diffusion, and possibly also to the different solubility of the different carbon isotopes in such a foil.[25,30] A similar isotope effect is found in samples 4d and 4e. The concentration of ^{13}C in sample

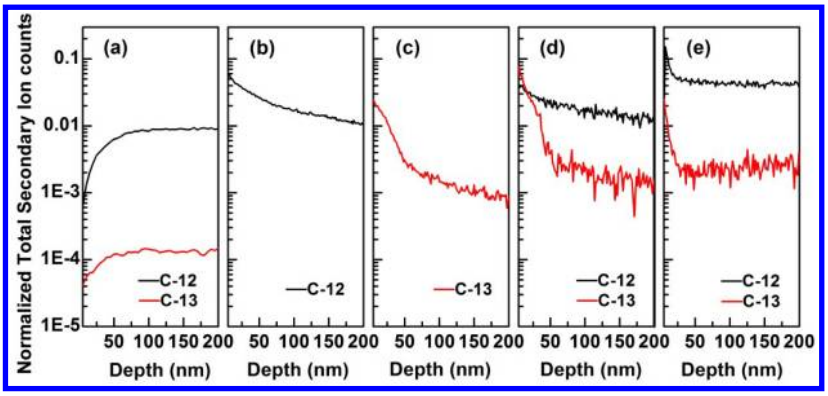

Figure 4. (a) The depth profiles of background ^{12}C and ^{13}C in Cu−Ni alloy foil without carbon deposition. (b,c) The depth profiles of ^{12}C and ^{13}C in Cu−Ni alloy foil for the two samples grown with only ^{12}C or only ^{13}C deposition, respectively. (d,e) The depth profiles of ^{12}C and ^{13}C in Cu−Ni alloy foil for the two samples with opposite isotope-deposition orders.

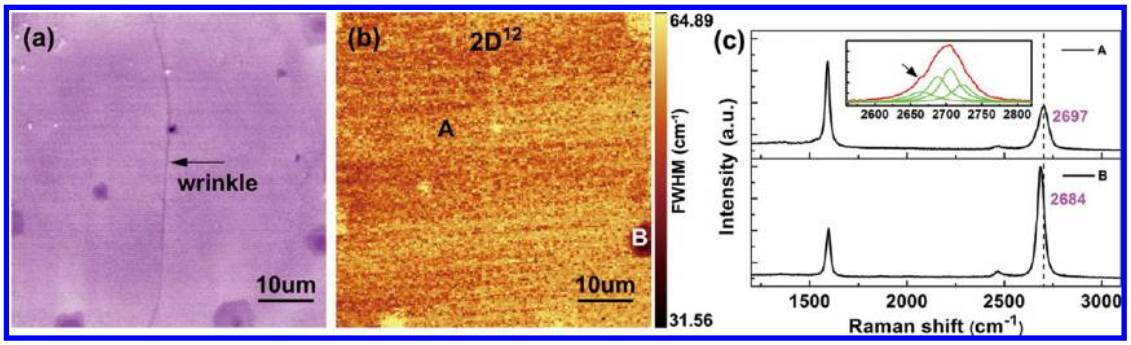

Figure 5. (a) Optical microscope image of bilayer graphene transferred onto a 285 nm SiO_2/Si substrate. (b) Raman map of the fwhm of ^{12}C-2D ($2D^{12}$, 2650−2750 cm^{-1}) band from the same area in panel a. (c) Raman spectra from the positions marked by A and B in panel b.

4d is about twice that of ^{12}C near the surface, but becomes lower than that of ^{12}C as the depth passes 20 nm. In sample 4e, the profiles of ^{12}C and ^{13}C almost parallel each other, but the ^{12}C penetrates further into the alloy foil, leading to about an order of magnitude higher concentration than that of ^{13}C. Considering that the solubility of carbon in our Cu−Ni alloy is about 0.01 wt % at 1000 °C,[31] it takes carbon atoms that are distributed within around 8 nm of the surface of the Cu−Ni alloy foil to form a complete monolayer graphene film. Integrating the TOF-SIMS data within 8 nm of the surface, the content of ^{12}C in sample 4b is about 1.5 times higher than that of ^{13}C in sample 4c, and the content of ^{12}C in sample 4e is about 8 times higher than that of ^{13}C in sample 4d. These results suggest that the concentration gradient of ^{12}C at the surface of the Cu−Ni alloy is higher than that of ^{13}C, though *in situ* temperature-dependent TOF-SIMS data were not possible as they are limited by the measurement technique. The higher diffusion coefficient and concentration gradient of ^{12}C results in a higher diffusion flux than that of ^{13}C according to Fick's law, and these factors dominate the graphene growth rate at the Cu−Ni alloy surface. Moreover, the carbon concentration gradient at the surface also depends on the diffusion of ^{12}C and ^{13}C atoms as the carbon source, thus, the diffusion coefficient difference of ^{12}C and ^{13}C could be the major factor for the higher growth rate of ^{12}C-graphene.

According to our previous work,[16] the precipitation process is strongly dependent on the cooling rate of the substrate. Thus, the isotopic growth process described here was used to control the ratio of ^{12}C and ^{13}C in graphene by changing only the cooling rate (see Supporting Information Figure S2).

Since the carbon deposition temperature, time, diffusion coefficient, and cooling rate can all influence the graphene coverage or the isotopic composition, this work provided us a path to obtain multilayer graphene with different isotopic compositions in each layer. As shown in Figure S3 (see Supporting Information), we synthesized a graphene monolayer of nearly pure ^{13}C with adlayers having 84.3% ^{12}C and 15.7% ^{13}C. Such isotopically engineered graphene may possess some new physical properties, for example, the thermal transport.[32]

In addition, for all the samples above, the submonolayer and adlayer graphene islands are almost hexagonal in shape, with maximum diameter measured to be around 25 and 10 μm, respectively. For each island, only one set of diffraction patterns was present in transmission electron microscopy (TEM)

selected area electron diffraction (SAED) measurements, indicative of single crystal structure. Dozens of submonolayer islands were measured, and a typical SAED image is shown in the Supporting Information Figure S4.

By controlling the growth conditions, we obtained submonolayer and monolayer graphene and, also, we synthesized bilayer graphene on Cu−Ni alloy. Generally, the turbostratic graphene is due to the dislocations between two graphene layers,[33] and a slower crystal growth rate yields fewer crystalline dislocations. We found that a slow cooling rate favors AB-stacked bilayer graphene, because at this condition the slow precipitation of carbon yields slow growth. Therefore, a cooling rate of 5 °C/min was used for growing AB-stacked bilayer graphene. A low methane flow rate and a long deposition time can further improve the uniformity of bilayer graphene. Figure S5 (in Supporting Information) shows the optical images of two samples grown at 1050 °C and a cooling rate of 5 °C/min. Sample S5-a and sample S5-b were synthesized with 10 sccm CH_4 for 40 min, and with 5 sccm CH_4 for 70 min, respectively. Compared with sample S5-a, the proportion of bilayer graphene coverage of sample S5-b is greatly improved from 52.1% to 82.2%. We suggest that it is because a more uniform distribution of carbon in Cu−Ni alloy was formed under a lower methane flow rate and longer heating time. Favorable growth conditions for bilayer graphene are as follows: 2 sccm H_2 and 3 sccm CH_4 (P_{Me} = 45 mTorr) at 1050 °C for 100 min, and a cooling rate of 5 °C/min. A typical bilayer graphene film transferred onto a SiO_2/Si substrate is shown in Figure 5a. Over 96% of the 80 × 80 μm^2 area has the same contrast, which suggests uniform thickness. In Figure 5b, the fwhm of the Raman 2D band was mapped and shows that most of the area has a fwhm within 45−52 cm^{-1}, except for some multilayer graphene islands. These islands have a 2D band fwhm of around 60 cm^{-1} except for the region B, where the fwhm is around 32 cm^{-1}. Raman spectra of region A and B (marked in Figure 5b) are shown in Figure 5c. In region A, the D band is undetectable, and the intensity ratio of I_G/I_{2D} is around 2. The 2D band is blue-shifted about 13 cm^{-1} with respect to monolayer graphene, and the fwhm is 48 cm^{-1} with a distinct shoulder present in the left side of the peak (marked by the black arrow in the inset of Figure 5c). Also, four Lorentzian peaks centered at 2658, 2688, 2706, and 2721 cm^{-1} fit the 2D band very well.[34−36] These results suggest that most of the area in Figure 5a is bilayer graphene with strong coupling between the layers.[34−37] In region B, the I_G/I_{2D} ratio is around 0.5 and the 2D band fwhm is 32 cm^{-1} without obvious broadening, which are the typical characteristics of a weak or noncoupling multilayer graphene.

The stacking structure of the bilayer graphene was studied by TEM.[38] We transferred the film onto a TEM grid and located the edge between monolayer and double-layer graphene by SEM. As shown in Figure 6a, region B is brighter than A, indicating more graphene layers. A high resolution TEM image (Figure 6b) was taken at region B, with the folded area showing a fringe spacing of about 0.34 nm and corresponding to bilayer graphene.[39] SAED patterns of regions A and B, and their diffraction intensities along the red lines are displayed in Figure 6 panels c and d, respectively. Only one set of diffraction patterns with 6-fold symmetry is found for each region. For region A, the intensity of the first-order diffraction is higher than that of the second-order, indicating monolayer graphene. For region B, the diffraction patterns have the same orientation as that of region A, but the first-order diffraction has lower intensity than the second-order, which suggests that the double-layer graphene in region B is AB-stacked.[35,38]

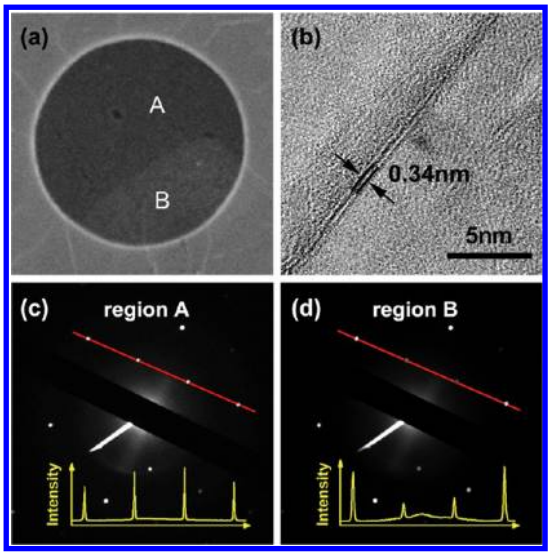

Figure 6. (a) SEM image of a graphene film transferred onto a TEM grid, with monolayer graphene in region A and bilayer graphene in region B. (b) high resolution TEM image taken in region B, with the distinct fingerprints showing an interlayer spacing of about 0.34 nm. (c and d) The SAED patterns and the corresponding intensities along the red lines measured in region A and B, respectively, implying monolayer and AB-stacked bilayer graphene.

CONCLUSION

A hot wall CVD system was used to synthesize graphene films on "90−10" Cu−Ni alloy foils. By sequentially introducing isotopic carbon, graphene with randomly mixed isotopes was formed and detected by Raman spectroscopy. This suggests a surface precipitation mechanism of graphene growth on Cu−Ni alloy. The growth parameters were studied and it was found that a higher carbon deposition temperature, longer deposition time, and slower cooling rate resulted in greater graphene coverage on this Cu−Ni alloy foil. Compared with ^{13}C-graphene, greater coverage of ^{12}C-graphene in identical growth conditions was also

observed and this indicates that the carbon diffusion coefficient greatly affects the graphene growth. Based on the surface precipitation growth model presented here, large-area, uniform bilayer graphene was obtained, with Raman and TEM results strongly indicating it had an AB-stacked structure.

METHODS

A hot wall CVD system with a horizontal tube furnace was used to synthesize graphene thin films. Polycrystalline Cu−Ni foils (120 μm-thick; weight percent, 88.00% Cu, 9.90% Ni, 0.44% Mn, 1.54% Fe, and 0.10% Zn, All Metal Sales, Inc.) were cut into 10 mm $\times$50 mm pieces and loaded into the tube as the metal substrates. A vacuum background of about 0.1 mTorr was reached in the tube before carbon deposition. The substrates were heated to 1050 °C and held for 30 min under 2 sccm H_2 (Air Gas Inc. 99.999%) to remove the surface oxide before growth. $^{12}CH_4$ (Air Gas, 99.999%) and $^{13}CH_4$ (Cambridge Isotopes, 99.2% pure) were used as the gaseous carbon source. The process was similar to that used for growing graphene on Cu foil.[11] The growth parameters such as deposition temperature, time, and cooling rate were controlled to obtain ^{12}C- or ^{13}C-graphene with different coverage. The graphene thin films were transferred by poly(methyl methacrylate) (PMMA) onto either SiO_2/Si (285 nm SiO_2) substrates for Raman measurements, or TEM grids (with quantifoil holey carbon film) for TEM studies.[11]

SEM images of the samples were taken with an FEI Quanta-600 FEG Environmental SEM using a beam voltage of 30 kV. The carbon isotopes in graphene and the number of stacking layers were determined by a confocal microprobe Raman system (WITec Alpha300, 100$\times$ N.A., 532 nm excitation laser, ~6 mW).[40,41] The Raman laser beam size was about 250 nm, and a 200 nm step size was applied in mapping to cover the whole scanning region. The TOF-SIMS spectra were acquired on a TOF.SIMS5 instrument (ION-TOF GmbH, Germany, 2010). Cs^+ and O_2^+ ions at 1 kV were used as the sputter beams to obtain negative and positive secondary ions, respectively, and 30 kV Bi^+ ions composed the analysis beam. TEM images were obtained on a JEOL2010F TEM operating at an accelerating voltage of 200 kV, using an acquisition time of 1 s.[42] A Gatan image filter and multiscan digital CCD camera were used for the image acquisition with a resolution of 1024 $\times$ 1024 pixels and binning of 1 $\times$ 1.

Conflict of Interest: The authors declare no competing financial interest.

Acknowledgment. We gratefully appreciate support from the National Science Foundation (Grant No. 1006350 and DMR-0923096), the Office of Naval Research, SWAN NRI, the National "973" Program of China (Grant Nos. 2012CB619301 and 2011CB925600), the National Natural Science Foundation of China (Grant Nos. 90921002, and 60827004). We also acknowledge the TOF-SIMS facility and the Texas Materials Institute at University of Texas at Austin for the data acquisition and interpretation.

Supporting Information Available: Two control experiments for the estimation of residual carbon impurities within the substrate, Figure S1; the effect of cooling rate on graphene coverage and isotopic composition, Figure S2; isotopically engineered graphene layers, Figure S3; TEM SAED measurements of submonolayer graphene, Figure S4; the growth of bilayer graphene with different methane flow rates and deposition times, Figure S5. This material is available free of charge *via* the Internet at http://pubs.acs.org.

REFERENCES AND NOTES

1. Dreyer, D. R.; Ruoff, R. S.; Bielawski, C. W. From Conception to Realization: An Historial Account of Graphene and Some Perspectives for Its Future. *Angew. Chem., Int. Ed.* **2010**, *49*, 9336–9344.
2. Katsnelson, M. I. Graphene: Carbon in Two Dimensions. *Mater. Today* **2006**, *10*, 20–27.
3. May, J. W. Platinum Surface LEED Rings. *Surf. Sci.* **1969**, *17*, 267–270.
4. Novoselov, K. S.; Geim, A. K.; Morozov, S. V.; Jiang, D.; Zhang, Y.; Dubonos, S. V.; Grigorieva, I. V.; Firsov, A. A. Electric Field Effect in Atomically Thin Carbon Films. *Science* **2004**, *306*, 666–669.
5. Geim, A. K.; Novoselov, K. S. The Rise of Graphene. *Nat. Mater.* **2007**, *6*, 183–191.
6. Zhang, Y.; Tan, Y. W.; Stormer, H. L.; Kim, P. Experimental Observation of the Quantum Hall Effect and Berry's Phase in Graphene. *Nature* **2005**, *438*, 201–204.
7. Luo, Z.; Yu, T.; Shang, J.; Wang, Y.; Lim, S.; Liu, L.; Gurzadyan, G. G.; Shen, Z.; Lin, J. Large-Scale Synthesis of Bi-layer Graphene in Strongly Coupled Stacking Order. *Adv. Funct. Mater.* **2011**, *21*, 911–917.
8. Samarakoon, D. K.; Wang, X. Q. Tunable Band Gap in Hydrogenated Bilayer Graphene. *ACS Nano* **2010**, *4*, 4126–4130.
9. Yan, K.; Peng, H.; Zhou, Y.; Li, H.; Liu, Z. Formation of Bilayer Bernal Graphene: Layer-by-Layer Epitaxy *via* Chemical Vapor Deposition. *Nano Lett.* **2011**, *11*, 1106–1110.
10. Lee, S.; Lee, K.; Zhong, Z. Wafer Scale Homogeneous Bilayer Graphene Films by Chemical Vapor Deposition. *Nano Lett.* **2010**, *10*, 4702–4707.
11. Li, X.; Cai, W.; An, J.; Kim, S.; Nah, J.; Yang, D.; Piner, R.; Velamakanni, A.; Jung, I.; Tutuc, E.; *et al.* Large-Area Synthesis of High-Quality and Uniform Graphene Films on Copper Foils. *Science* **2009**, *324*, 1312–1314.
12. Li, X.; Cai, W.; Jung, I.; An, J.; Yang, D.; Velamakanni, A.; Piner, R.; Colombo, L.; Ruoff, R. S. Synthesis, Characterization, and Properties of Large-Area Graphene Films. *ECS Trans.* **2009**, *19*, 41–52.
13. Reina, A.; Jia, X.; Ho, J.; Nezich, D.; Son, H.; Bulovic, V.; Dresselhaus, M. S.; Kong, J. Large Area, Few-Layer Graphene Films on Arbitrary Substrates by Chemical Vapor Deposition. *Nano Lett.* **2009**, *9*, 30–35.
14. Stoddart, D. R. Retrospect and Prospect of Aldabra Research. *Nature* **1969**, *221*, 1004–1006.
15. Fedoseev, D. V.; Vnukov, S. P.; Derjaguin, B. V. Physicochemical Theory of Graphite Growth from Hydrocarbons. *Carbon* **1979**, *17*, 453–458.
16. Chen, S.; Cai, W.; Piner, R. D.; Suk, J. W.; Wu, Y.; Ren, Y.; Kang, J.; Ruoff, R. S. Synthesis and Characterization of Large-Area Graphene and Graphite Films on Commercial Cu−Ni Alloy Foils. *Nano Lett.* **2011**, *11*, 3519–3525.
17. Dai, B.; Fu, L.; Zou, Z.; Wang, M.; Xu, H.; Wang, S.; Liu, Z. Rational Design of a Binary Metal Alloy for Chemical Vapour Deposition Growth of Uniform Single-Layer Graphene. *Nat. Commun.* **2011**, *2*, 522.
18. Li, X.; Cai, W.; Colombo, L.; Ruoff, R. S. Evolution of Graphene Growth on Ni and Cu by Carbon Isotope Labeling. *Nano Lett.* **2009**, *9*, 4268–4272.
19. López, G. A.; Mittemeijer, E. J. The Solubility of C in Solid Cu. *Scr. Mater.* **2004**, *51*, 1–5.
20. Yamane, T.; Okubo, H.; Hisayuki, K.; Oki, N.; Konishi, M.; Komatsu, M.; Minamino, Y.; Koizumi, Y.; Kiritani, M.; Kim, S. J. Solid Solubility of Carbon in Copper Mechanically Alloyed. *J. Mater. Sci. Lett.* **2001**, *20*, 259–260.
21. Fan, S.; Liu, L.; Liu, M. Monitoring the Growth of Carbon Nanotubes by Carbon Isotope Labelling. *Nanotechnology* **2003**, *14*, 1118–1123.
22. Fick., A. Ueber Diffusion. *Ann. Phys.* **1855**, *170*, 59–86.
23. Marchese, M.; Lorenzi, G. D.; Jacucci, G.; Flynn, C. P. Jump Dynamics and the Isotope Effect in Solid-State Diffusion. *Phys. Rev. Lett.* **1986**, *57*, 3280–3283.
24. Jacucci, G.; Lorenzi, G. D.; Marchese, M.; Flynn, C. P.; Toller, M. Theory of Classical Diffusion Jumps in Solids. II. Isotope Effect and First-Order Anharmonic Terms. *Phys. Rev. B* **1987**, *36*, 3086–3094.

25. Lässer, R.; Klatt, K. H. Solubility of Hydrogen Isotopes in Palladium. *Phys. Rev. B* **1983**, *28*, 748–758.
26. O'leary, M. H. Measurement of the Isotope Fractionation Associated with Diffusion of Carbon-Dioxide in Aqueous Solution. *J. Phys. Chem.* **1984**, *88*, 823–825.
27. Zeebe, R. E.; Bijma, J.; Wolf-Gladrow, D. A. A Diffusion-Reaction Model of Carbon Isotope Fractionation in Foraminifera. *Mar. Chem.* **1999**, *64*, 199–227.
28. Cheng, J.; Winograd, N. Depth Profiling of Peptide Films with TOF-SIMS and a C_{60} Probe. *Anal. Chem.* **2005**, *77*, 3651–3659.
29. Peled, E.; Tow, D. B.; Merson, A.; Gladkich, A.; Burstein, L.; Golodnitsky, D. Composition, Depth Profiles and Lateral Distribution of Materials in the SEI Built on HOPG-TOF SIMS and XPS Studies. *J. Power Sources* **2001**, *97*−*98*, 52–57.
30. Powell, G. L. Solubility of Hydrogen and Deuterium in a Uranium−Molybdenum Alloy. *J. Phys. Chem.* **1976**, *80*, 375–381.
31. Nicholson, M. E. The Solubility of Carbon in Nickel−Copper Alloys at 1000 °C. *Trans. Metall. Soc. AIME* **1962**, *224*, 533–535.
32. Chen, S.; Wu, Q.; Mishra, C.; Kang, J.; Zhang, H.; Cho, K.; Cai, W.; Balandin, A. A.; Ruoff, R. S. Thermal Conductivity of Isotopically Modified Graphene. *Nat. Mater.* **2012**, *11*, 203–207.
33. Robertson, A. W.; Bachmatiuk, A.; Wu, Y. A.; Schäffel, F.; Rellinghaus, B.; Büchner, B; Rümmeli, M. H.; Warner, J. H. Atomic Structure of Interconnected Few-Layer Graphene Domains. *ACS Nano* **2011**, *5*, 6610–6618.
34. Ni, Z.; Wang, Y.; Yu, T.; Shen, Z. Raman Spectroscopy and Imaging of Graphene. *Nano Res.* **2008**, *1*, 273–291.
35. Ferrari, A. C.; Meyer, J. C.; Scardaci, V.; Casiraghi, C.; Lazzeri, M.; Mauri, F.; Piscanec, S.; Jiang, D.; Novoselov, K. S.; Roth, S.; *et al.* Raman Spectrum of Graphene and Graphene Layers. *Phys. Rev. Lett.* **2006**, *97*, 187401.
36. Malard, L. M.; Pimenta, M. A.; Dresselhaus, G.; Dresselhaus, M. S. Raman Spectroscopy in Graphene. *Phys. Rep.* **2009**, *473*, 51–87.
37. Frank, O.; Mohr, M.; Maultzsch, J.; Thomsen, C.; Riaz, I.; Jalil, R.; Novoselov, K. S.; Tsoukleri, G.; Parthenios, J.; Papagelis, K.; *et al.* Raman 2D-Band Splitting in Graphene: Theory and Experiment. *ACS Nano* **2011**, *5*, 2231–2239.
38. Meyer, J. C.; Geim, A. K.; Katsnelson, M. I.; Novoselov, K. S.; Booth, T. J.; Roth, S. The Structure of Suspended Graphene Sheets. *Nature* **2007**, *446*, 60–63.
39. Yan, Z.; Peng, Z.; Sun, Z.; Yao, J.; Zhu, Y.; Liu, Z.; Ajayan, P. M.; Tour, J. M. Growth of Bilayer Graphene on Insulating Substrates. *ACS Nano* **2011**, *5*, 8187–8192.
40. Ji, H.; Hao, Y.; Ren, Y.; Charlton, M.; Lee, W. H.; Wu, Q.; Li, H.; Zhu, Y.; Wu, Y.; Piner, R.; Ruoff, R. S. Graphene Growth Using a Solid Carbon Feedstock and Hydrogen. *ACS Nano* **2011**, *5*, 7656–7661.
41. Hao, Y.; Wang, Y.; Wang, L.; Ni, Z.; Wang, Z.; Wang, R.; Koo, C. K.; Shen, Z.; Thong, J. T. L. Probing Layer Number and Stacking Order of Few-Layer Graphene by Raman Spectroscopy. *Small* **2010**, *6*, 195–200.
42. Wu, Y.; Jiang, W.; Ren, Y.; Cai, W.; Lee, W. H.; Li, H.; Piner, R. D.; Pope, C. W.; Hao, Y.; Ji, H. Tuning the Doping Type and Level of Graphene with Different Gold Configurations. *Small* **2012**, published online July 24, 2012, doi: 10.1002/smll.201200520.